Redistribution of Nucleoside Transporters to the Cell Membrane Provides a Novel Approach for Imaging Thymidylate Synthase Inhibition by Positron Emission Tomography

Meg Perumal,[1] Radhakrishna G. Pillai,[1] Henryk Barthel,[1,2] Julius Leyton,[1] John R. Latigo,[1] Martin Forster,[3] Fraser Mitchell,[3] Ann L. Jackman,[3] and Eric O. Aboagye[1]

[1]Molecular Therapy Group, Faculty of Medicine, Imperial College London, Hammersmith Hospital, London, United Kingdom; [2]Department of Nuclear Medicine, University of Leipzig, Leipzig, Germany; and [3]Section of Medicine, Institute of Cancer Research, Surrey, United Kingdom

Abstract

Thymidylate synthase (EC 2.1.1.45) is a key enzyme for the *de novo* synthesis of DNA and as such a target for anticancer drug development. There is a need to develop noninvasive methods for assessing thymidylate synthase inhibition in tumors. The aim of this study was to assess the potential of 3′-deoxy-3′-[^{18}F]fluorothymidine ([^{18}F]FLT) positron emission tomography (PET) for early measurement of thymidylate synthase inhibition and to elucidate the cellular mechanisms involved. Radiation-induced fibrosarcoma-1 tumor-bearing mice were injected with a single i.p. dose of the thymidylate synthase inhibitor 5-fluorouracil (5-FU; 165 mg/kg) and imaged by [^{18}F]FLT-PET at 1 to 2 hours after treatment. Deoxyuridine, thymidine kinase 1 (cytoplasmic thymidine kinase; EC2.7.1.21), and ATP levels in excised tumors were measured. Cellular assays for membrane transport were also done. There was a 1.8-fold increase in the 60-minute [^{18}F]FLT tumor/heart radioactivity ratio in drug-treated mice compared with vehicle controls (P = 0.0016). Plasma and tumor deoxyuridine levels increased significantly but thymidine kinase and ATP levels were unchanged. Whole-cell assays implicated a (low level) functional role for the type-1 equilibrative nucleoside transporter (ENT). There was an increase in type-1 ENT-binding sites per cell from 49,110 in untreated cells to 73,142 (P = 0.03) in cells treated with 10 μg/mL 5-FU for 2 hours, without a change in transporter affinity (P = 0.41). We conclude that [^{18}F]FLT-PET can be used to measure thymidylate synthase inhibition as early as 1 to 2 hours after treatment with 5-FU by a mechanism involving redistribution of nucleoside transporters to the plasma membrane. (Cancer Res 2006; 66(17): 8558-64)

Introduction

Thymidylate synthase (EC 2.1.1.45) is a critical enzyme for DNA replication because it catalyses the *de novo* synthesis of thymidine monophosphate (TMP), a key nucleotide precursor for DNA synthesis. Due to its central role in DNA synthesis, thymidylate synthase remains an exploitable target for anticancer drug development. Pyrimidines, such as 5-fluorouracil (5-FU) in combination with leucovorin, a reduced folate that stabilizes the binding of 5-FU to thymidylate synthase, have been used for several decades in the treatment of gastrointestinal and other cancers (1–3). More recently oral 5-FU prodrugs, such as capecitabine, have been developed (1, 4, 5). In addition to these pyrimidines, inhibitors that are structural analogues of 5,10-methylenetetrahydrofolate, a cosubstrate of thymidylate synthase, generally referred to as antifolates, have been developed. These include raltitrexed, permetrexed, nolatrexed, and BGC 9331 (ZD9931; refs. 6–9). Whereas the above agents inhibit both normal tissue and tumor thymidylate synthase, new antifolates, such as BGC 638 and BGC 945, are targeted to tumors via the α-folate receptor, leading to selective inhibition of tumor thymidylate synthase (6, 10, 11).

Quantification of thymidylate synthase inhibition in tumors currently relies on measurement of biochemical changes that accompany thymidylate synthase inhibition (2, 7). For instance, thymidylate synthase inhibition leads to an increase in intracellular pools of the thymidylate synthase substrate dUMP and its corresponding nucleoside 2′-deoxyuridine; thus, pharmacodynamic effects of thymidylate synthase inhibitors have been assessed by measuring elevation of this nucleoside in the patient's plasma (7, 8). However, elevated plasma 2′-deoxyuridine is mainly a marker of global thymidylate synthase inhibition in proliferating cells (i.e., not tumor specific). Positron emission tomography (PET) imaging of thymidylate synthase biochemistry is a strategy that may provide more specific information at the tumor site and could have important use in the development of the next generation of thymidylate synthase inhibitors.

The positron emitting radiotracer 2-[^{11}C]thymidine, a substrate for thymidine kinase 1 (TK1; cytoplasmic thymidine kinase; EC2.7.1.21 ref. 12), a key enzyme in salvage pathway for producing TMP (13), has been assessed for its potential for imaging thymidylate synthase inhibition (14). In that study, patients treated with nolatrexed and scanned 1 hour after drug administration had an increase in tumor 2-[^{11}C]thymidine-related radioactivity levels that correlated with area under the plasma nolatrexed concentration versus time curve (14). It was hypothesized that inhibition of the *de novo* pathway will lead to enhanced use of TMP produced via the salvage pathway and hence 2-[^{11}C]thymidine uptake. The radiotracer 2-[^{11}C]thymidine is, however, not an ideal PET marker because it is rapidly metabolized *in vivo* (15). In the present report, we investigated the feasibility of the more metabolically stable thymidine analogue, 3′-deoxy-3′-[^{18}F]fluorothymidine ([^{18}F]FLT; ref. 16), to image thymidylate synthase inhibition. We showed for the first time that [^{18}F]FLT-PET can be used very early to image inhibition of thymidylate synthase *in vivo* by a mechanism involving redistribution of nucleoside transporters to the plasma membrane.

Requests for reprints: Eric O. Aboagye, Molecular Therapy Group, Faculty of Medicine, Imperial College London, Clinical Sciences Centre, Medical Research Council Cyclotron Building, Hammersmith Hospital, Du Cane Road, London W12 0NN, United Kingdom. Phone: 44-20-8383-3759; Fax: 44-20-8383-2027; E-mail: eric.aboagye@imperial.ac.uk.

doi:10.1158/0008-5472.CAN-06-0898

Materials and Methods

Radiochemicals. [^{18}F]FLT was produced on-site by Hammersmith Imanet Ltd. (Medical Research Council Cyclotron Building, Hammersmith Hospital, London, United Kingdom). It was prepared by radiofluoridation of the 2,3′-anhydro-5′-*O*-(4,4′-dimethoxytrityl)-thymidine precursor as has been described previously (17). [Methyl-^{3}H]thymidine ([^{3}H]TdR; 925 GBq/mmol, 37 MBq/mL) and [2-^{3}H]adenine ([^{3}H]adenine; 777 GBq/mmol, 37 MBq/mL) were purchased from GE Healthcare UK Ltd. (Little Chalfont, Buckinghamshire, United Kingdom). [^{3}H]FLT (174 GBq/mmol, 37 MBq/mL) and [^{3}H]nitrobenzyl mercaptopurine ribonucleoside (NBMPR), also known as [^{3}H]*S*-(*p*-nitrobenzyl)-6-thioinosine (555 GBq/mmol, 37 MBq/mL), were purchased from Moravek Biochemicals, Inc. (Brea, CA).

Cell lines and tumors. Radiation-induced fibrosarcoma-1 (RIF-1) cells (18) were cultured in RPMI 1640 (Life Technologies, Strathclyde, United Kingdom) supplemented with 10% fetal bovine serum (Sigma, Poole, United Kingdom) and antibiotics in a 5% CO_2 incubator at 37°C. Exponentially growing cells were used for the *in vitro* radiotracer studies or inoculated into 6- to 8-week-old-male C3H/Hej mice obtained from Harlan UK Ltd. (Bicester, United Kingdom). Tumors were induced by inoculation of 5×10^5 cells s.c. on the back of the mice. All animal work was done by licensed investigators in accordance with the United Kingdom's "Guidance on the Operation of Animals (Scientific Procedures) Act 1986" (HMSO, London, United Kingdom, 1990) and in full compliance with government regulations and guidelines on the welfare of animals in experimental neoplasia (19). Tumors were selected for PET imaging studies when they reached 5 to 8 mm in diameter.

PET scanning and image analysis. Mice were scanned on a dedicated small animal PET scanner (quad-HIDAC; Oxford Positron Systems, Weston-on-the-Green, United Kingdom; refs. 18, 20, 21). Before scanning, the mice were treated with either PBS (control) or 5-FU at a single i.p. dose of 165 mg/kg body weight and scanned at 1 to 2 hours after drug injection. For scanning, anesthesia was induced with isofluorane/O_2/N_2O and the tail veins of the mice were cannulated. The animals were placed within a thermostatically controlled bed and positioned prone within the scanner. The bed was calibrated to provide a mouse rectal temperature of ~37°C. A bolus injection of [^{18}F]FLT (2.96-3.7 MBq; 80-100 μCi) was given i.v. via the tail vein cannula and scanning commenced. Dynamic emission scans were acquired in list-mode format over 60 minutes. The acquired data were then sorted into 0.5-mm sinogram bins and 19 time frames ($0.5 \times 0.5 \times 0.5$ mm voxels; 4×15, 4×60, and 11×300 seconds) for image reconstruction, which was done by filtered back projection using a two-dimensional Hamming filter (cutoff 0.6). The image data-sets obtained were transferred to a SUN workstation (Ultra 10; SUN Microsystems, Santa Clara, CA) and visualized using the Analyze software (version 6.0; Biomedical Imaging Resource, Mayo Clinic, Rochester, MN). Cumulative images of the dynamic data composed of 0 to 1 minute after injection and 30 to 60 minutes after injection were used for visualization of radiotracer uptake and to define the regions of interest (ROI) on heart (mainly blood pool) and tumors, respectively. ROIs were defined on five tumor and five heart slices (each 0.5 mm thickness). The count densities were averaged for each ROI at each of the 19 time points to obtain a time versus radioactivity curve (TAC) for the ROIs. Tumor TAC was normalized to that of heart at each of the time points to obtain the normalized uptake value (NUV). The [^{18}F]FLT-PET data from heart were used as internal input function for normalizing tumor data because it comprises mainly of blood radioactivity (18). The NUV at 60 minutes after injection (NUV_{60}), the area under the NUV curve (AUC) calculated as the integral of NUV from 0 to 60 minutes, and the fractional retention of tracer (FRT), the radioactivity at 60 minutes relative to that at 2.5 minutes, were used for comparisons. FRT is a useful variable in that it indicates the proportion of radiotracer delivered to the tumor that is retained. It therefore normalizes tumor [^{18}F]FLT uptake to delivery.

Analysis of tumor 2′-deoxyuridine levels. To confirm that thymidylate synthase was inhibited by 5-FU, 2′-deoxyuridine levels were assessed by high-performance liquid chromatography (HPLC). Plasma and RIF-1 tumors were taken from mice treated with PBS or 165 mg/kg 5-FU at 2 hours after injection and immediately snap frozen in liquid nitrogen. This time point was selected to coincide with the imaging assay. Plasma samples (150 μL) were initially prepared using perchlorate protein precipitation; after neutralization and centrifugation, the supernatant was purified by solid-phase extraction. Whole (weighed) tumor samples were homogenized and the homogenate was treated similar to plasma samples. After evaporation to dryness using a vacuum centrifuge, the samples were reconstituted for analysis by reverse-phase HPLC as described previously (22). 2′-Deoxyuridine was separated on a C18 stationary phase with a mobile phase comprising 0.1% trifluoroacetic acid and detected at 267 nm using a UV photodiode array detector. 2′-Deoxyuridine losses from sample preparation were estimated by measuring the recovered activity of [5-^{3}H]2′-deoxyuridine spiked into blank plasma or tumor samples. Chromatographic peak areas for the samples were compared with a calibration curve; data were expressed as micromole per liter and nanomole per gram for plasma and tumors, respectively.

Analysis of tumor TK1 protein and cofactor levels. TK1 protein and cofactor (ATP) were assessed by Western blot and bioluminescence assays, respectively. RIF-1 tumors were excised from mice treated with PBS or 165 mg/kg 5-FU at 2 hours after injection and snap frozen in liquid nitrogen. Tumors were pulverized in liquid nitrogen and homogenized in ice-cold PBS using an Ultra-Turrax homogenizer (IKA, Staufen, Germany). The samples were then centrifuged at $800 \times g$ (for 30 minutes at 4°C) and supernatants were analyzed for protein content using a commercial bicinchoninic acid (BCA) protein assay kit (Perbio Science, Cheshire, United Kingdom). Aliquots of the supernatants (containing 30 μg protein) were mixed with equivalent volumes of native Tris-glycine sample buffer (Invitrogen Life Science, Paisley, United Kingdom) and separated on a precast Tris-glycine (4-20%) gel (Invitrogen). Western blot analysis was done as described previously (18, 20). For quantification of band intensities, the films were scanned using a GS-710 Calibrated Imaging Densitometer (Bio-Rad Laboratories, Hertfordshire, United Kingdom) and analyzed with the Quantity One software (version 4.0.3; Bio-Rad Laboratories). ATP levels were determined by a bioluminescence assay as described previously (18, 20) using the same supernatants used for the Western blots above. A calibration curve was prepared from ATP standards, which were provided with the ATP assay kit.

Incorporation of radioactivity into DNA. RIF-1 cells were cultured in full growth medium as above and treated with 1 or 10 μg/mL 5-FU dissolved in PBS or an equal volume of PBS for 2 hours. After drug treatment, the cells were washed and incubated with 0.185 MBq tritiated thymidine ([^{3}H]TdR) or [^{3}H]FLT for 1 hour. The cells were washed and scraped into plastic tubes. The cellular protein content of whole cells was assayed by a commercial BCA protein assay kit and used for normalization of radioactivity levels in DNA (assuming no losses in the DNA assay) on different days. The cells were centrifuged. DNA was isolated from whole-cell pellet using the AquaPure Genomic Isolation kit (Bio-Rad Laboratories, Hercules, CA). Hydrated DNA samples were placed in opaque 24-well plates (Perkin-Elmer, Beaconsfield, United Kingdom) and left to dry. Aliquots (500 μL) of scintillant (Microscint-40; Perkin-Elmer) were added to each well and the radioactivity in each well was counted on a β-counter (TopCount NXT, Packard Instruments, Meriden, CT). Data were quench corrected and expressed as counts per minute (cpm)/mg protein.

Cellular membrane transport inhibition assays. To determine the mechanism of whole-cell plasma membrane transport, cell uptake studies were done with [^{18}F]FLT in the presence or absence of various known inhibitors (23). RIF-1 cells were cultured as above and treated with full growth medium containing PBS or 10 μg/mL of 5-FU for 2 hours. After drug treatment, the cells were washed and trypsinized. The effect of trypsin was blocked with full growth medium. The cells were washed again and suspended in HBSS (Sigma). Cells (2×10^6) were preincubated for 15 minutes in HBSS buffer containing PBS (control) or an inhibitor of nucleoside or nucleobase transport (and phosphorylation), including 20 μmol/L nitrobenzylthioguanosine (NBTG), 20 μmol/L dipyridamole, 2 mmol/L thymidine, 2 mmol/L uridine, 2 mmol/L adenine, and 2 mmol/L thymine; total incubation volume of 1 mL. The cells were then incubated with 1.8 to 3.7 MBq [^{18}F]FLT at room temperature (~20°C) for 1 hour with mild shaking. At the end of the incubation period, the reaction was quickly stopped by adding 5 mL ice-cold PBS and centrifuged at $500 \times g$ for 5 minutes. The supernatant was removed; the cells were washed once and resuspended in 100 μL of 2.5× lysis buffer (10% sodium carbonate,

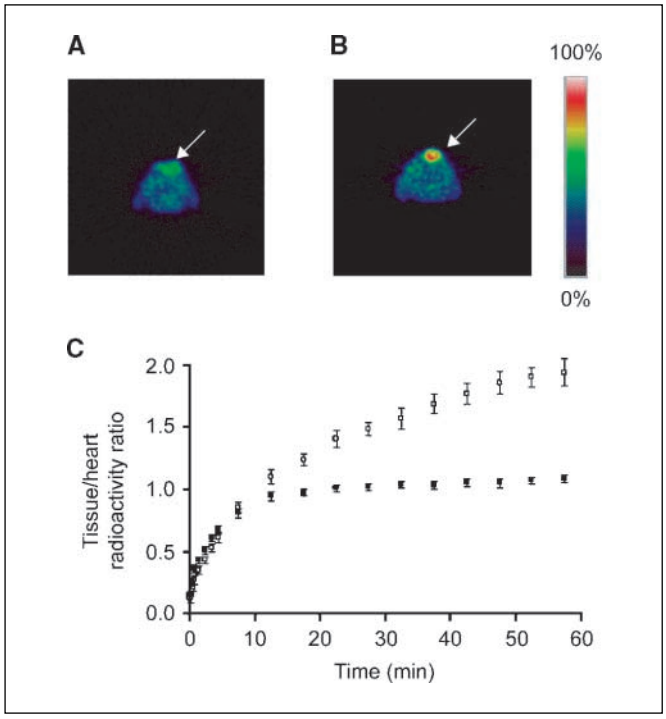

Figure 1. Typical 0.5-mm transverse [^{18}F]FLT-PET slices through the thoracic region at the level of the maximum tumor diameter of a RIF-1 tumor–bearing mouse treated with PBS (*control*; *A*) and a RIF-1 tumor–bearing mouse treated with 5-FU (*B*). *Arrows,* tumor. Note color bar. *C,* summary of [^{18}F]FLT kinetics in control (●) and 5-FU-treated (○) RIF-1 tumors. Tumor-bearing mice were treated with PBS or 5-FU at a dose of 165 mg/kg i.p. and scanned at 1 to 2 hours after injection. For each mouse, tumor/heart radioactivity ratios from five slices were averaged at each of the 19 time points. *Points,* mean tumor/heart ratios from eight control mice and five 5-FU-treated mice; *bars,* SE.

0.5% sodium dodecyl sulphate, 0.5mol/L sodium hydroxide) until the cells were fully disintegrated. The solution was carefully transferred into opaque 24-well plates and air dried. Aliquots (500 μL) of scintillant were added and the radioactivity was counted using a microplate β-counter (TopCount). Data were expressed as a percentage of the radioactivity added (percent cpm of dose solution per 2×10^6 cells). For comparison, the uptake of [^{3}H]TdR in 10 μg/mL 5-FU-treated cells was determined as for [^{18}F]FLT above in the presence and absence of NBTG and expressed as a percentage of the mean uptake in uninhibited cells.

To confirm or rule out the involvement of nucleobase transport, transport studies in PBS-treated cells or 10 μg/mL 5-FU-treated cells were done as above for [^{18}F]FLT but with 0.185 MBq [^{3}H]adenine as radiotracer. In these studies, 2 mmol/L thymidine was used to saturate phosphorylation of adenine.

Kinetics of nucleoside transport. In these studies, exponentially growing RIF-1 cells were treated for 2 hours with PBS or 5-FU at concentrations of 1 or 10 μg/mL. Single cells prepared by trypsinization were suspended in HBSS with mild shaking. To assess plasma membrane NBMPR-sensitive nucleoside transporter-binding sites on RIF-1 cells, 2×10^6 cells were incubated with 0.1, 0.25, 0.5, 1, 2, 4, 8, 16 nmol/L [^{3}H]NBMPR in HBSS. The total incubation volume was 400 μL and the studies were carried out at room temperature (~20°C) for 60 minutes (equilibrium binding). In parallel experiments to assess nonspecific binding, equal numbers of cells were preincubated with 20 μmol/L of the specific inhibitor, NBTG, for 15 minutes and then incubated with [^{3}H]NBMPR at the same concentration range. At the end of the incubation, the reaction was quickly stopped by adding 5 mL ice-cold Na^+ buffer [150 mmol/L NaCl, 5 mmol/L Tris-HCl (pH 7.4)] and the mixture was centrifuged at $500 \times g$ for 5 minutes. The supernatant was removed and the cells were washed once and resuspended in 100 μL lysis buffer until they were fully disintegrated. The solution was carefully transferred into opaque 24-well plates and air dried, and the radioactivity was counted (TopCount). Specific binding (binding sites per cell) was defined as the difference in [^{3}H]NBMPR content in the presence and absence of NBTG. The maximal binding (B_{max}; the number of transporters) and the concentration of ligand required to reach half-maximal binding (K_D; affinity) were determined by curve fitting using the Prism software, version 4.03 (GraphPad, San Diego, CA). Data were fitted to the equation: $Y = B_{max} \times X / (K_D + X)$, where Y and X are the specific binding and [^{3}H]NBMPR concentration in nmol/L, respectively.

Statistics. Statistical analyses were done using the Prism software, version 4.03 (GraphPad). Differences between PBS- and 5-FU-treated groups were tested for significance using the Student's t test for unpaired data. Two-tailed Ps ≤0.05 were considered significant.

Results

The accumulation of [^{18}F]FLT in RIF-1 tumors increases early after 5-FU treatment. We have shown previously that [^{18}F]FLT uptake decreases at 24 and 48 hours after a single i.p. dose of 5-FU (165 mg/kg), whereby the post-5-FU [^{18}F]FLT uptake correlated with histologically assessed proliferation. Figure 1*A* and *B* shows the localization of [^{18}F]FLT in RIF-1 tumors 1 to 2 hours after treatment with PBS or 5-FU at the same dose used previously. Localization of radioactivity was seen in the PBS-treated tumor (Fig. 1*A*) that was qualitatively enhanced by 5-FU treatment at 1 to 2 hours (Fig. 1*B*). Quantitative assessment of the time course of [^{18}F]FLT uptake in RIF-1 tumors after i.v. injection of the radiotracer also showed increased uptake (Fig. 1*C*). The two TACs in this case were visually different after ~15 minutes. A summary of the kinetic components calculated from the TACs are depicted in Table 1. All variables, including the NUV_{60}, FRT, and AUC, were significantly higher in the 5-FU-treated mice compared with vehicle controls (Table 1). We also examine whether thymidylate synthase was inhibited under the conditions used. Both plasma and tumor

Table 1. Summary of PET pharmacokinetics for PBS- and 5-FU-treated mice together with corresponding deoxyuridine levels

	NUV_{60}	FRT	AUC (activity ratio × min)	Plasma deoxyuridine level (μmol/L)	Tumor deoxyuridine level (nmol/g)
PBS (n)	1.08 ± 0.03 (8)	2.62 ± 0.17 (8)	57.42 ± 1.48 (8)	2.38 ± 0.37 (4)	10.66 ± 2.50 (4)
5-FU (n)	1.93 ± 0.11 (5)	5.85 ± 0.46 (5)	85.68 ± 3.69 (5)	4.21 ± 0.47 (4)	24.82 ± 3.14 (4)
Significance (5-FU vs PBS)	0.0016	0.0016	0.0016	0.02	0.01

NOTE: Data are mean ± SE (number of tumors). NUV_{60}, FRT, and AUC were determined from [^{18}F]FLT-PET TACs obtained at 1 to 2 hours after 5-FU administration as described in Materials and Methods. Deoxyuridine levels were determined by HPLC as described in Materials and Methods.

2′-deoxyuridine levels, surrogate measures of thymidylate synthase inhibition (7, 8), were significantly increased after 5-FU treatment by ~2-fold (Table 1).

The early 5-FU-induced accumulation of [^{18}F]FLT in tumors is not due to enhanced TK1 protein, ATP levels, or incorporation of [^{18}F]FLT into DNA. We have attributed previously an increase in radiolabeled thymidine uptake after treatment with different thymidylate synthase inhibitors to enhanced salvage kinetics in an attempt of cells to overcome the block in TMP production via the *de novo* pathway (14, 24). Because tumor uptake of [^{18}F]FLT increased *in vivo* after thymidylate synthase inhibition, we examined key salvage pathway events, including TK1 levels, ATP levels, and incorporation of radioactivity into DNA, which might explain the increased [^{18}F]FLT uptake. Figure 2*A* and *B* shows TK1 and ATP levels in PBS- and 5-FU-treated tumor homogenates. These variables did not increase as expected. In contrast, there were nonsignificant decreases in both protein and cofactor levels. This indicates that the increased uptake of [^{18}F]FLT into tumors after thymidylate synthase inhibition occurs under normal levels of TK1 and ATP. Examination of thymidine incorporation into DNA was done with tritiated FLT [^{3}H]FLT using [^{3}H]TdR as a positive control. For [^{3}H]TdR, a significant increase in radiotracer uptake into cells was seen at two 5-FU concentrations ($P \leq 0.03$; Fig. 2*C*). The amount of radioactivity in DNA was 26.5% of that in whole cells. In contrast, there was no change in [^{3}H]FLT uptake into DNA (Fig. 2*D*); the amount of radioactivity in DNA was 0.2% of that in whole cells. This indicates that thymidylate synthase inhibition does not increase [^{18}F]FLT uptake into the DNA pool.

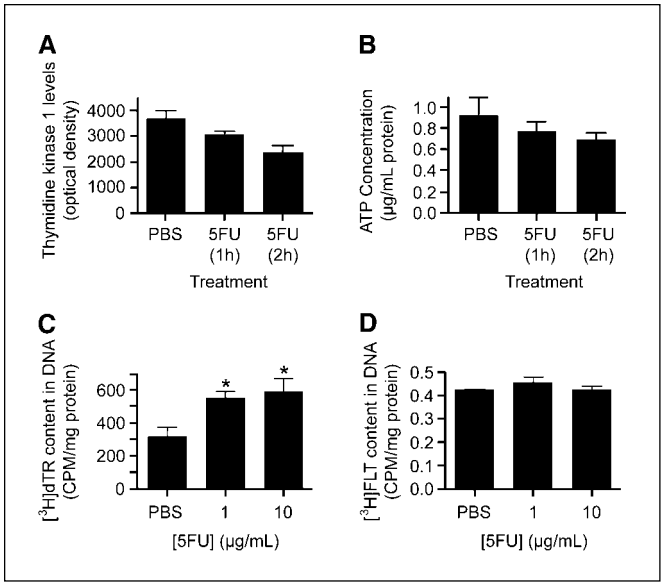

Figure 2. TK1 protein levels (*A*) and ATP concentration (*B*) in excised PBS- and 5-FU-treated tumors. TK1 protein was analyzed by Western blot and densitometry and expressed as absorbance units (arbitrary); control levels were not significantly different from treated levels; $P = 0.89$ and 0.40 for the 1- and 2-hour treatment groups, respectively. ATP concentration was analyzed by a bioluminescence method; control levels were not significantly different from treated levels; $P = 0.11$ and 0.06 for the 1- and 2-hour treatment groups, respectively. DNA content of [^{3}H]TdR (*C*) and [^{3}H]FLT (*D*) in PBS- and 5-FU-treated cultured RIF-1 cells. The cells were treated with 1 or 10 μg/mL 5-FU for 2 hours and washed off of drug. This was followed by 1 hour of incubation with [^{3}H]TdR or [^{3}H]FLT and extraction of DNA as described in Materials and Methods. *Columns,* mean cpm normalized to whole-cell protein content ($n = 4$); *bars,* SE. *, $P \leq 0.03$. Note the different *Y* axis scales.

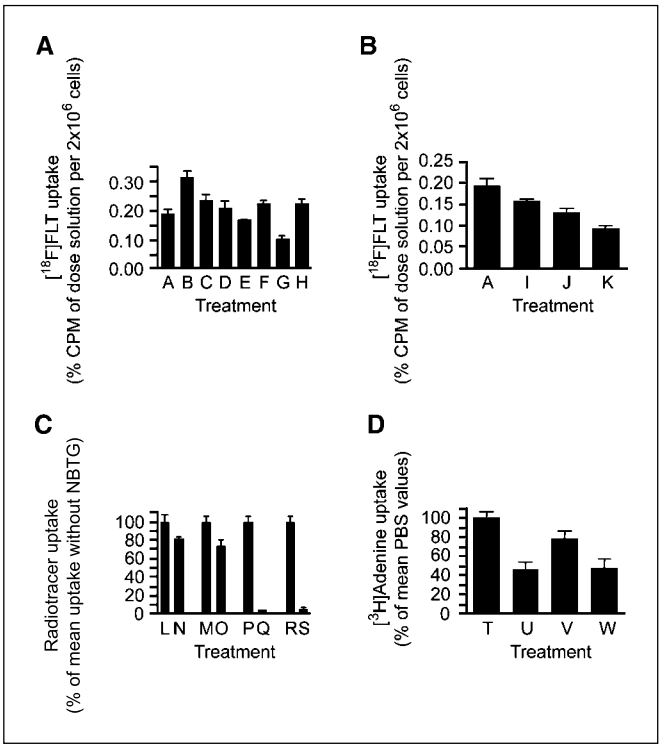

Figure 3. Mechanism of [^{18}F]FLT cell membrane transport in RIF-1 cells growing in culture. Exponentially growing adherent cells that were treated with 5-FU at 10 μg/mL or with PBS (control) for 2 hours were washed and trypsinized, and 2 million cells were incubated with [^{18}F]FLT, [^{3}H]TdR, or [^{3}H]adenine in HBSS buffer for 1 hour in the presence or absence of nucleoside or nucleobase transport inhibitors. For inhibitor studies, cells were preincubated with the membrane transport inhibitors for 15 minutes. The cells were washed to remove free radioactivity with ice-cold PBS and assayed for the amount of radioactivity by scintillation counting ($n = 3$-4 experiments for each condition). *A,* effect of membrane transport inhibitors on [^{18}F]FLT uptake: *columns A* and *B,* untreated and 5-FU-treated cells, respectively; *columns C, D, E, F, G,* and *H,* 5-FU-treated cells that were preincubated with 20 μmol/L NBTG, 20 μmol/L dipyridamole, 2 mmol/L thymidine, 2 mmol/L uridine, 2 mmol/L adenine, and 2 mmol/L thymine, respectively. *Columns,* mean [^{18}F]FLT uptake per 2 million cells expressed as a percentage of radioactivity of the dose solution; *bars,* SE. *B,* effect of selected inhibitors on [^{18}F]FLT uptake in drug-free (PBS treated) cells: *columns A, I, J,* and *K,* control, 20 μmol/L NBTG, 2 mmol/L thymidine, and 2 mmol/L adenine, respectively. *Columns,* mean [^{18}F]FLT uptake per 2 million cells expressed as a percentage of radioactivity of the dose solution; *bars,* SE. *C,* comparison of [^{18}F]FLT and [^{3}H]TdR with respect to inhibition of nucleoside transport with and without 5-FU treatment. *Columns,* mean radiotracer uptake; *bars,* ± SE. Each uptake data set is expressed as a percentage of the respective mean uptake in the absence of the inhibitor NBTG (*columns L, N, P,* and *R*). *Columns L* and *M* and *columns N* and *O,* uptake values for [^{18}F]FLT in the absence and presence of 5-FU, respectively; *Columns P* and *Q* and *columns R* and *S,* uptake values for [^{3}H]TdR in the absence and presence of 5-FU, respectively. *D,* comparison of [^{3}H]adenine uptake in PBS-treated (*columns T* and *U*) and 5-FU-treated cells (*columns V* and *W*) in the absence (*columns T* and *V*) and presence (*columns U* and *W*) of thymidine, respectively. Data are expressed as a percentage of the mean uptake in *column T*. $P \leq 0.05$, statistically significant for PBS or 5-FU controls versus inhibitor-treated comparisons in (*A* and *C*), for adenine and thymidine comparisons in (*B*), and for PBS versus 5-FU, PBS versus PBS-thymidine pretreated, and 5-FU versus 5-FU-thymidine pretreated comparisons in (*D*).

Inhibitor studies indicate a role for equilibrative nucleoside transporter type 1. To examine the role of membrane transport, the uptake of [^{18}F]FLT was studied in the presence or absence of known inhibitors of nucleoside or nucleobase transport. As in RIF-1 tumors, *in vitro* [^{18}F]FLT uptake in RIF-1 cells increased significantly after 5-FU treatment (Fig. 3*A*). The increased uptake was reduced by pretreatment with equilibrative nucleoside transport (ENT) inhibitors NBTG [type 1 ENT (ENT1) selective]

and dipyridamole [ENT1 and type 2 ENT (ENT2) selective]. The lack of a differential in [^{18}F]FLT uptake between these two inhibitors suggested that only ENT1 was inhibited or that the cells lacked ENT2. Thymidine and uridine, which (in addition to ENT) are substrates for the concentrative sodium-dependent nucleoside transporters, also decreased the 5-FU-induced [^{18}F]FLT uptake. A significant decline in uptake was also seen with the nucleobase transport inhibitors, adenine and thymine. Without 5-FU treatment, decreases in [^{18}F]FLT uptake were seen with thymidine and adenine (Fig. 3*B*); there was a slight decrease with NBTG but that was not statistically significant. This indicates that the decreases in 5-FU-induced [^{18}F]FLT uptake seen in Fig. 3*A* may in part be due to a decrease in baseline (uninduced) uptake. To confirm that ENT1 was involved in the 5-FU-induced [^{18}F]FLT uptake, we examined induced versus uninduced uptake of the natural ENT1 substrate [^{3}H]TdR in the presence or absence of NBTG (Fig. 3*C*). The uptake of [^{3}H]TdR in RIF-1 cells was almost completely blocked by NBTG in uninduced and 5-FU-induced cells (Fig. 3*C*). Figure 3*C* also shows that ENT1-dependent transport was lower in magnitude for [^{18}F]FLT compared with [^{3}H]TdR. Thymine can be converted to thymidine and mask uptake studies. Adenine uptake can be confounded by TK1-dependent phosphorylation. Hence, we studied [^{3}H]adenine uptake in uninduced and 5-FU-induced cells using thymidine to saturate TK1-dependent phosphorylation. Figure 3*D* shows that [^{3}H]adenine uptake decreased after 5-FU treatment. In thymidine preinhibited cells, there was no difference in [^{3}H]adenine uptake between PBS- and 5-FU-treated cells. These studies indicate that nucleobase transport may not be important in 5-FU-induced [^{18}F]FLT uptake.

ENT1 levels increase with 5-FU treatment. Because of a 1:1 stoichiometry between inhibitor and membrane-associated transporter levels, kinetic analysis of cell uptake with [^{3}H]NBMPR permits the number of membrane-associated ENT (predominantly ENT1) transporters and affinity of the transporter to be measured (25–27). Figure 4 shows the kinetics of [^{3}H]NBMPR uptake in PBS- and 5-FU-treated RIF-1 cells. The curves revealed a 5-FU concentration–dependent increase in the specific uptake of [^{3}H]NBMPR (i.e., the difference between the uptake of [^{3}H]NBMPR in the presence and absence of NBTG). A summary of the number of transporters (B_{max}) and transporter affinity (K_D) derived from this kinetic analysis is shown in Table 2. There was a 1.5-fold increase in number of transporters on the membrane after treatment of cells with 10 μg/mL 5-FU for 2 hours, without a change in transporter affinity. A nonsignificant increase in B_{max} was seen at 1 μg/mL 5-FU; K_D was not significantly different from control values in this case too.

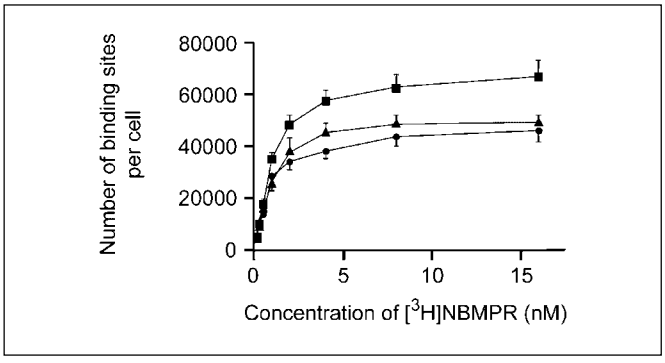

Figure 4. Effect of 5-FU on the binding kinetics of [^{3}H]NBMPR to RIF-1 cells. [^{3}H]NBMPR kinetics were used to determine the maximum binding (B_{Max}), which reflect the number of ENT1 receptors, and affinity (K_D) as described in Materials and Methods. *Points,* mean binding sites per cell (n = 5 independent experiments); *bars,* SE. *Curves,* a 5-FU-induced increase in receptor-binding sites. A summary of the various B_{Max} and K_D values are presented in Table 2.

Table 2. The effect of 5-FU on [^{3}H]NBMPR kinetics in RIF-1 cells growing in culture

	B_{Max} (no. binding sites per cell)	K_D (nmol/L)	Significance (5-FU versus PBS)
PBS	49,101 ± 4,013	1.031 ± 0.16	—
5-FU (1 μg/mL)	54,980 ± 3,811	1.263 ± 0.43	B_{Max}, 0.28; K_D, 1.00
5-FU (10 μg/mL)	73,142 ± 6,849	1.198 ± 0.13	B_{Max}, 0.03; K_D, 0.41

NOTE: Under the conditions used, [^{3}H]NBMPR kinetics reflect the number and affinity of ENT1 nucleoside transporters on the cell membrane. Data are mean ± SE.

Discussion

We have shown for the first time that [^{18}F]FLT-PET can be used to measure thymidylate synthase inhibition *in vivo* and defined the biochemical mechanism at the cellular level. Thymidylate synthase is a key enzyme for the *de novo* synthesis of DNA and as such a target for anticancer drug development. Currently the most widely established pharmacodynamic marker used for monitoring the efficacy of thymidylate synthase inhibition is an increase in plasma 2′-deoxyuridine, a consequence of increased intracellular dUMP in proliferating tissues throughout the body (7, 8, 28). Although easily accessible, this marker does not measure thymidylate synthase inhibition specifically at the tumor site and thus may be insensitive for the next generation of tumor-specific thymidylate synthase inhibitors. A PET imaging approach may overcome this limitation. We have developed [^{18}F]FLT-PET for this purpose. [^{18}F]FLT is a stable analogue of thymidine. 2-[^{11}C]thymidine uptake has been shown to increase following AG337 administration (14). We subsequently showed that this phenomenon occurred in different cell types and following AG337 and 5-FU treatment but not after treatment with cisplatin that does not inhibit thymidylate synthase (24). In that study, the thymidylate synthase induced increases of [^{3}H]TdR uptake occurred within 1 to 6 hours and classic decreases in [^{3}H]TdR uptake resulting from inhibition of cell proliferation were observed at 24 and 48 hours after treatment (24). In a recent study by Gibbs et al. (11), tumor [^{125}I]2′-deoxyuridine uptake was shown to increase after treatment of mice with the novel thymidylate synthase inhibitors BGC 638 and BGC 945. Thus, increase in nucleoside uptake after thymidylate synthase inhibition may be a general phenomenon that could be exploited to assess pharmacodynamics of thymidylate synthase inhibitors. Furthermore, it is not cell type dependent as the effects are seen in mouse and human cells, including RIF-1, HT29, and KB cells (11, 24).

[^{18}F]FLT has superior *in vivo* stability compared with 2-[^{11}C]thymidine and [^{124}I]iododeoxyuridine (29). Hence, we assessed the feasibility of using this radiotracer for imaging thymidylate synthase inhibition. Marked increase in [^{18}F]FLT-PET imaging end points together with marked increases in both plasma and tumor 2′-deoxyuridine were seen 1 to 2 hours after 5-FU treatment *in vivo*. We have proposed in previous studies that the mechanism of

increased radiolabeled thymidine uptake following thymidylate synthase inhibition may involve increased use of the salvage pathway for producing DNA in an attempt of cells to overcome the block in TMP production via the *de novo* pathway (14, 24). This assertion was based on the use of radiolabeled thymidine, which is readily incorporated into DNA. In the present study, we showed that [^{3}H]TdR incorporation into DNA was enhanced by 5-FU treatment and that the DNA component comprised a substantial part of whole-cell uptake (26.5%). The proportion of [^{3}H]FLT in DNA was only 0.2% that of whole cell and did not change after 5-FU treatment. This finding indicated that the mechanisms of retention of the two radiotracers were different. It also indicated that enhanced incorporation of thymidine analogues into DNA to overcome the block of the *de novo* pathway per se was not responsible for the general increase in nucleoside uptake. Examination of TK1 and ATP levels, the enzyme system responsible for the initial commitment of thymidine into the salvage pathway, showed no change in levels that could account for the increase in [^{18}F]FLT uptake early after 5-FU treatment. Lastly, we examined membrane transport of [^{18}F]FLT and showed that [^{18}F]FLT was transported by ENT1, albeit at low levels compared with [^{3}H]TdR. The low substrate specificity of [^{18}F]FLT for ENT1 even under conditions of 5-FU induction may be due to the lack of a 3′-OH group, which seems to be important for the transport of nucleoside analogues by ENT1 (30, 31).

Interestingly, we discovered that treatment of RIF-1 cells with 10 μg/mL 5-FU increased plasma membrane NBMPR-sensitive nucleoside transporter (predominantly ENT1) binding sites from 49,101 in untreated cells to 73,142 ($P = 0.03$). Thus, although a poor substrate, [^{18}F]FLT is transported by ENT1 under conditions of thymidylate synthase inhibition due to the large increase in numbers of plasma membrane ENT1 transporters. The lack of a change in transporter K_D ($P \geq 0.41$) with 5-FU treatment indicates that there was no modification in affinity of the transporter and/or no recruitment of other ENT transporter subtypes. Total 100,000 × *g* membrane fractions prepared from PBS- and 5-FU-treated RIF-1 tumors did not show differences in [^{3}H]NBMPR binding; ENT1 mRNA levels of control and 10 μg/mL 5-FU-treated RIF-1 cells measured by quantitative real-time PCR were not different from each other.[4] These findings indicate that increased salvage kinetics induced by thymidylate synthase inhibition is not due to increased transcription or translation of ENT1 but is largely or exclusively due to redistribution of the transporter from the intracellular compartment of cells to the plasma membrane. ENT1 is predominantly localized on the plasma membrane of both human and mouse cells (32, 33). In addition to the plasma membrane, ENT1 is known to localize to mitochondria (30). Whether it is the mitochondrial pool that redistributes to the membrane remains to be determined. It is unlikely that a third ENT family member, ENT3, which is insensitive to NBMPR and has been shown to localize in the intracellular/lysosomal pool (33), will be responsible for the observed effects. Furthermore, the reason why thymidylate synthase inhibitors (11, 14, 24, 34), but not other anticancer agents, affect radiolabeled nucleoside uptake through ENT1 in this manner remains to be elucidated.

In general, the [^{18}F]FLT-PET methodology should allow early pharmacodynamic effects of thymidylate synthase inhibitors to be studied in preclinical models and in patients. Such studies will involve a baseline [^{18}F]FLT-PET scan followed by another [^{18}F]FLT-PET scan soon after drug treatment. The time course of [^{18}F]FLT-PET changes will depend on the pharmacokinetics of the thymidylate synthase inhibitor, dose, and mechanism of interaction of the inhibitor with thymidylate synthase (i.e., rate and persistence of thymidylate synthase inhibition). A limitation of the technology is the relatively short length of time that PET measurements will continue to show increased [^{18}F]FLT uptake, reflecting inhibition of thymidylate synthase inhibition, rather than a decrease in [^{18}F]FLT uptake, reflecting inhibition of cell proliferation. Our previous studies with 5-FU and AG337 indicate that this time window is ≥6 and ≤24 hours in cultured cells (24). *In vivo* studies at the same dose of 5-FU used here shows a reduction in [^{18}F]FLT uptake at 24 and 48 hours (18). Mathematical modeling to calculate [^{18}F]FLT permeability product surface area may allow the thymidylate synthase inhibition effect, which relates to nucleoside transport to be measured at 24 hours or longer. In the use of [^{18}F]FLT-PET for monitoring the antiproliferative activity of thymidylate synthase inhibitors, as opposed to its use for determining thymidylate synthase inhibitory activity reported here, the early increases might be interpreted as a "flare" effect and confound the [^{18}F]FLT-PET studies. We will caution the use of [^{18}F]FLT-PET for monitoring antiproliferative activity of 5-FU-containing regimen during the dosing period (soon after a bolus dose or during and soon after continuous infusion); the same applies to chronic dosing with other thymidylate synthase inhibitors. We will speculate from our previous *in vitro* and *in vivo* studies (18, 24) that [^{18}F]FLT-PET-based antiproliferation measurements could be done a few days after 5-FU administration.

Imaging methods could accelerate drug development by providing information on whether adequate levels of drug are achieved, whether the drug hits its intended target, and whether the expected biological activity is achieved (35). [^{18}F]FLT-PET could be used to determine if thymidylate synthase inhibitors modulate their intended molecular target in tumors and normal tissues. In summary, [^{18}F]FLT-PET imaging can be used to measure thymidylate synthase inhibition in tumors *in vivo* very early after drug administration. The cellular mechanism by which [^{18}F]FLT-PET measures thymidylate synthase involves redistribution of nucleoside transporters to the plasma membrane.

Acknowledgments

Received 3/13/2006; revised 6/2/2006; accepted 6/15/2006.

Grant support: Cancer Research United Kingdom grant CA2536/A4892 and Medical Research Council (core funding).

The costs of publication of this article were defrayed in part by the payment of page charges. This article must therefore be marked *advertisement* in accordance with 18 U.S.C. Section 1734 solely to indicate this fact.

We thank the Wellcome Trust for award of the Joint Infrastructure fund that enabled us to purchase the HIDAC PET scanner.

[4] M. Perumal, R.G. Pillai, E.O. Aboagye, unpublished data.

References

1. Meyerhardt JA, Mayer RJ. Systemic therapy for colorectal cancer. N Engl J Med 2005;352:476–87.
2. Peters GJ, van de Wilt CL, van Groeningen CJ, Smid K, Meijer S, Pinedo HM. Thymidylate synthase inhibition after administration of fluorouracil with or without leucovorin in colon cancer patients: implications for treatment with fluorouracil. J Clin Oncol 1994; 12:2035–42.
3. Pinedo HM, Peters GF. Fluorouracil: biochemistry and pharmacology. J Clin Oncol 1988;6:1653–64.

4. Meropol NJ. Oral fluoropyrimidines in the treatment of colorectal cancer. Eur J Cancer 1998;34:1509–13.
5. Walko CM, Lindley C. Capecitabine: a review. Clin Ther 2005;27:22–44.
6. Jackman AL, Theti DS, Gibbs DD. Antifolates targeted specifically to the folate receptor. Adv Drug Deliv Rev 2004;56:1111–25.
7. Ford HER, Mitchell F, Cunningham D, et al. Patterns of elevation of plasma 2′-deoxyuridine, a surrogate marker of thymidylate synthase (TS) inhibition, after administration of two different schedules of 5-fluorouracil and the specific TS inhibitors raltitrexed (Tomudex) and ZD9331. Clin Cancer Res 2002;8:103–9.
8. Rafi I, Boddy AV, Calvete JA, et al. Preclinical and phase I clinical studies with the nonclassical antifolate thymidylate synthase inhibitor nolatrexed dihydrochloride given by prolonged administration in patients with solid tumours. J Clin Oncol 1998;16:1131–41.
9. Webber S, Bartlett CA, Boritzki TJ, et al. AG337, a novel lipophilic thymidylate synthase inhibitor: *in vitro* and *in vivo* preclinical studies. Cancer Chemother Pharmacol 1996;37:509–17.
10. Theti DS, Bavetsias V, Skelton LA, et al. Selective delivery of CB300638, a cyclopenta[g]quinazoline-based thymidylate synthase inhibitor into human tumor cell lines overexpressing the a-isoform of the folate receptor. Cancer Res 2003;63:3612–8.
11. Gibbs DD, Theti DS, Wood N, et al. BGC 945, a novel tumor-selective thymidylate synthase inhibitor targeted to α-folate receptor-overexpressing tumors. Cancer Res 2005;65:11721–8.
12. Lin PF, Zhao SY, Ruddle FH. Genomic cloning and preliminary characterisation of the human thymidine kinase gene. Proc Natl Acad Sci U S A 1983;80:6528–32.
13. Weber G, Nagai M, Natsumeda Y. Regulation of *de novo* and salvage pathways in chemotherapy. Adv Enzyme Regul 1991;31:45–67.
14. Wells P, Aboagye E, Gunn RN, et al. 2-[^{11}C]thymidine positron emission tomography as an indicator of thymidylate synthase inhibition in patients treated with AG337. J Natl Cancer Inst 2003;95:675–82.
15. Wells P, Gunn RN, Alison M, et al. Assessment of proliferation *in vivo* using 2-[^{11}C]thymidine positron emission tomography in advanced intra-abdominal malignancies. Cancer Res 2002;62:5698–702.
16. Shields AF, Grierson JR, Dohmen BM, et al. Imaging proliferation *in vivo* with [F-18]FLT and positron emission tomography. Nat Med 1998;4:1334–6.
17. Cleji MC, Steel CJ, Brady F, Ell PJ, Pike VW, Luthra SK. An improved synthesis of 3′-deoxy-3′-[^{18}F]fluorothymidine ([UF]FLT) and the fate of the precursor 2,3′-anhydro-5′-*O*-(4,4′-dimethoxytrityl)-thymidine. J Labelled Compounds Radiopharm 2001;44:871–3.
18. Barthel H, Cleij MC, Collingridge DR, et al. 3′-Deoxy-3′-[^{18}F]fluorothymidine as a new marker for monitoring tumor response to anti-proliferative therapy *in vivo* with positron emission tomography. Cancer Res 2003;3:3791–8.
19. Workman P, Twentyman P, Balkwill F, et al. United Kingdom co-ordinating committee on cancer research (UKCCCR) guidelines for the welfare of animals in experimental neoplasia (second edition). Br J Cancer 1998;77:1–10.
20. Leyton J, Latigo JR, Perumal M, Dhaliwal H, He Q, Aboagye E. Early detection of tumour response to chemotherapy by 3′deoxy-3′-[^{18}F]fluorothymidine positron emission tomography: the effect of cisplatin on a fibrosarcoma tumour model *in vivo*. Cancer Res 2005;65:4202–10.
21. Barthel H, Perumal M, Latigo J, et al. The uptake of 3′deoxy-3′-[^{18}F]fluorothymidine into L5178Y tumors *in vivo* is dependent on thymidine kinase 1 protein and ATP levels. Eur J Nucl Med Mol Imaging 2005;32:257–63.
22. Mitchell F, Lynn S, Jackman AL. Modified high-performance liquid chromatography assay for the measurement of 2′-deoxyuridine in human plasma and its application to pharmacodynamic studies of antimetabolite drugs. J Chromatography B 2000;744:351–8.
23. Buursma AR, van Dillen IJ, van Waarde A, et al. Monitoring HSVtk suicide gene therapy: the role of [^{18}F]FHPG membrane transport. Br J Cancer 2004;91:2079–85.
24. Yau K, Price P, Pillai RG, Aboagye EO. Elevation of radiolabelled thymidine uptake in RIF-1 fibrosarcoma and HT29 colon adenocarcinoma cells after treatment with thymidylate synthase inhibitors. Eur J Nucl Med Mol Imaging. Epub 2006 March 28.
25. Lay-Beng GOH, Chee-Wee L. Reduction of equilibrative nitrobenzylthioinosine-sensitive nucleoside transporter in tamoxifen-treated MCF-7 cells: an oestrogen-reversible phenomenon. Biochem J 1997;327:31–6.
26. Boleti H, Coe IR, Baldwin SA, Young JD, Cass CE. Molecular identification of the equilibrative NBMPR-sensitive (es) Nucleoside transporter and demonstration of an equilibrative NBMPR-insensitive (ei) transport activity in human erythroleukemia (K562) cells. Neuropharmacology 1997;36:1167–79.
27. Hammond JR. Interaction of a series of draflazine analogues with equilibrative nucleoside transporters: species differences and transporter subtype selectivity. Naunyn Schmiedebergs Arch Pharmacol 2000;361:373–82.
28. de Jonge MJ, Punt CJ, Sparreboom A, et al. Phase I and pharmacologic study of oral ZD9331, a novel nonpolyglutamated thymidylate synthase inhibitor, in adult patients with solid tumors. J Clin Oncol 2002;20:1923–31.
29. Kenny LM, Aboagye EO, Price PM. Positron emission tomography imaging of cell proliferation in oncology. Clin Oncol (R Coll Radiol) 2004;16:176–85.
30. Lai Y, Tse C-M, Unadkat JD. Mitochondrial expression of the human equilibrative nucleoside transporter 1 (hENT1) results in enhanced mitochondrial toxicity of antiviral drugs. J Biol Chem 2004;279:4490–7.
31. Damaraju VL, Damaraju S, Young JD, et al. Nucleoside anticancer drugs: the role of nucleoside transporters in resistance to cancer chemotherapy. Oncogene 2003;22:7524–36.
32. Kiss A, Farah K, Kim J, Garriock RJ, Drysdale TA, Hammond JR. Molecular cloning and functional characterization of inhibitor-sensitive (mENT1) and inhibitor-resistant (mENT2) equilibrative nucleoside transporters from mouse brain. Biochem J 2000;352:363–72.
33. Baldwin SA, Yao SYM, Hyde RJ, et al. Functional characterisation of novel human and mouse equilibrative nucleoside transporters (hENT3 and mENT3) located in intracellular membranes. J Biol Chem 2005;280:15880–7.
34. Dittmann H, Dohmen BM, Kehlback R, et al. Early changes in [^{18}F]FLT uptake after chemotherapy: an experimental study. Eur J Nucl Med 2002;29:1462–9.
35. Workman P, Aboagye EO, Chung Y-L, et al. Minimally invasive pharmacokinetic and pharmacodynamic technologies in hypothesis-testing clinical trials of innovative therapies. J Natl Cancer Inst 2006;98:580–98.